A&A 540, A44 (2012)
DOI: 10.1051/0004-6361/201117896

Astronomy & Astrophysics

Rubidium, zirconium, and lithium production in intermediate-mass asymptotic giant branch stars

M. A. van Raai[1], M. Lugaro[2], A. I. Karakas[3], D. A. García-Hernández[4,5], and D. Yong[3]

[1] Sterrekundig Instituut, University of Utrecht, Postbus 80000, 3508 TA Utrecht, The Netherlands
e-mail: markvanraai@gmail.com
[2] Monash Centre for Astrophysics (MoCA), School of Mathematical Sciences, Monash University, 3800 Clayton Victoria, Australia
e-mail: maria.lugaro@monash.edu
[3] Research School of Astronomy and Astrophysics, Mt. Stromlo Observatory, Cotter Rd., Weston, ACT 2611, Australia
e-mail: [akarakas;yong]@mso.anu.edu.au
[4] Instituto de Astrofisica de Canarias, C/via Láctea s/n, 38200 La Laguna (Tenerife), Spain
e-mail: agarcia@iac.es
[5] Departamento de Astrofísica, Universidad de La Laguna (ULL), 38205 La Laguna, Spain

Received 17 August 2011 / Accepted 7 February 2012

ABSTRACT

Context. A recent survey of a large sample of Galactic intermediate-mass (>3 $M_{\odot}$) asymptotic giant branch (AGB) stars shows that they exhibit large overabundances of rubidium (Rb) up to 100–1000 times solar. In contrast, zirconium (Zr) is not enriched in these stars compared to its solar abundances. These observations set constraints on our theoretical notion of the *slow* neutron capture process (*s* process) that occurs inside intermediate-mass AGB stars. Lithium (Li) abundances are also reported for these stars. In intermediate-mass AGB stars, Li can be produced by proton captures occuring at the base of the convective envelope. For this reason the observations of Rb, Zr, and Li set complementary constraints on different processes occurring in the same stars.
Aims. We present predictions for the abundances of Rb, Zr, and Li as computed for the first time simultaneously in intermediate-mass AGB star models and compare them to the current observational constraints.
Methods. We calculate the Rb, Zr, and Li surface abundances for stellar models with masses between 3 and 6.5 $M_{\odot}$ and metallicities between 0.02 and 0.004.
Results. We find that the Rb abundance increases with increasing stellar mass, as is inferred from observations but we are unable to match the highest observed [Rb/Fe] abundances. Variations of the reaction rates of the neutron-capture cross sections involved with Rb production and the rate of the ^{22}Ne$(\alpha, n)^{25}$Mg reaction, responsible for neutron production inside these stars, yield only modest variations in the surface Rb content of ≈0.3 dex. Inclusion of a partial mixing zone (PMZ) to activate the ^{13}C$(\alpha, n)^{16}$O reaction as an additional neutron source yields significant enhancements in the Rb abundance. However this leads to Zr abundances that exceed the upper limits of the current observational constraints. If the third dredge-up (TDU) efficiency remains as high during the final stages of AGB evolution as during the earlier stages, we can match the lowest values of the observed Rb abundance range. We predict large variations in the Li abundance, which are observed. Finally, the predicted Rb production increases with decreasing metallicity, in qualitative agreement with observations of Magellanic Cloud AGB stars. However stellar models of $Z = 0.008$ and $Z = 0.004$ intermediate-mass AGB stars do not produce enough Rb to match the observed abundances.

Key words. nuclear reactions, nucleosynthesis, abundances – stars: AGB and post-AGB

1. Introduction

The elements heavier than iron are produced almost entirely by neutron-capture nucleosynthesis via the *s*(low) and the *r*(apid) processes, which are each responsible for roughly half of the cosmic abundances of these elements (Käppeler et al. 1989). During the *s* process timescales for neutron captures on unstable isotopes are typically lower than the decay timescales, which implies neutron densities $N_{\rm n} \sim 10^7$ cm^{-3}. Conversely, during the *r* process timescales for neutron captures on unstable isotopes are higher than decay timescales, which implies $N_{\rm n} > 10^{20}$ cm^{-3}. The element rubidium (Rb) is an example of an element that may have a significant *r*-process component, where ∼20–80% of its solar abundance has been ascribed to the *r* process. The exact value of this component depends on the *s*-process model used to calculate it, which can be parametric (Arlandini et al. 1999; Simmerer et al. 2004), stellar (Arlandini et al. 1999), or a chemical evolution model of the Galaxy (Travaglio et al. 2004). The *r* process contribution also depends on the uncertainties in the solar abundances and nuclear physics inputs (Goriely 1999). Zirconium (Zr) on the other hand is a typical element made by the *s* process, with ∼15–30% of its solar abundance ascribed to the *r* process. The *r* process is believed to occur in supernovae and/or neutron star mergers (Meyer 1994), while the *s*-process elements from Sr to Pb are produced in asymptotic giant branch (AGB) stars (Gallino et al. 1998).

The AGB is the final nuclear burning stage in the evolution of stars with initial masses in the range ≈0.8 to 8 $M_{\odot}$[1]. During the AGB the H-burning shell is responsible for the nuclear energy production most of the time, but every 10^{3-5} years or so the He shell ignites, driving convection throughout most of the He intershell, the He-rich region located between the H- and the

[1] Hereafter we refer to AGB stars with initial masses <3 $M_{\odot}$ as "low-mass" AGB stars, and to AGB stars with initial masses >3 $M_{\odot}$ as "intermediate-mass" AGB stars.

He-burning shells. This is known as a thermal pulse (TP). After a TP has occurred, at which time the H-burning shell lies dormant, the convective envelope extends inward and may reach the He intershell. This is known as the third dredge-up (TDU) and can occur periodically after each TP. The TDU mixes nuclear burning products from the He and H-burning shells to the stellar surface, increasing the abundance of carbon and in some cases leading to C > O at the stellar surface (Herwig 2005; Karakas & Lattanzio 2007; Lugaro & Chieffi 2011).

In the He intershell of AGB stars, neutrons for the *s* process can be released by the $^{13}C(\alpha, n)^{16}O$ reaction during the periods in-between TPs (interpulses) and by the $^{22}Ne(\alpha, n)^{25}Mg$ reaction in the convective TPs. The ^{13}C neutron source operates from $T \gtrsim 0.9 \times 10^8$ K and provides $N_n \sim 10^7$ cm^{-3}. In order to produce enough ^{13}C to match the enhancements of the *s*-process elements observed in AGB stars, it is assumed that some protons are mixed down into the He intershell at the deepest inward extent of each TDU episode (Gallino et al. 1998; Goriely & Mowlavi 2000; Busso et al. 2001). We refer to the region of the He-intershell that has undergone some partial mixing of protons as the "partially mixed zone" (PMZ). The protons are captured by the abundant ^{12}C producing ^{13}C and ^{14}N, which allows for the $^{13}C(\alpha, n)^{16}O$ reaction to be efficiently activated (Hollowell et al. 1990; Goriely & Mowlavi 2000; Lugaro et al. 2003). The ^{22}Ne neutron source requires $T > 3.5 \times 10^8$ K to be significantly activated and produces $N_n \approx 10^{10}$–10^{11} cm^{-3} in low-mass AGB stars and up to $N_n \approx 10^{13}$ cm^{-3} in intermediate-mass AGB stars (see Sect. 4). This is because temperatures in excess of 3×10^8 K are more easily reached during the TPs in intermediate-mass AGB stars (Iben 1975). The ^{13}C neutron source is active for a much longer period of time ($\sim 10^4$ yr) than the ^{22}Ne neutron source ($\sim$1 yr) and it produces a higher total amount of neutrons, even though with a lower neutron density.

The amount of Rb produced during the *s* process depends on the probability of the two unstable nuclei ^{85}Kr and ^{86}Rb capturing a neutron before decaying and acting as "branching points". The probability of this happening depends on the local neutron density (Beer & Macklin 1989). Figure 1 shows a section of the chart of the nuclides from Kr to Zr. Beer (1991) reported that, independently of the temperature, when ^{84}Kr captures a neutron, 50% of the flux proceeds to the ground state of ^{85}Kr (with half-life of 3934.4 days) and the other 50% proceeds to the metastable state of ^{85}Kr (with half-life of 4.480 h). Of the metastable ^{85}Kr, 20% decays to its ground state while the remaining 80% decays into ^{85}Rb. Effectively, 40% of $^{84}Kr+n$ results in the production of ^{85}Rb, whereas the other 60% results in the production of the ^{85}Kr ground state. The long decay time of the ^{85}Kr ground state allows it to capture another neutron to produce ^{86}Kr instead of ^{85}Rb, provided the neutron density is higher than $\approx 5 \times 10^8$ cm^{-3}. ^{86}Kr can also capture a neutron, producing ^{87}Kr which quickly decays (with a half-life of 76.3 min) into ^{87}Rb. The other unstable isotope in Fig. 1 is ^{86}Rb (with a half-life of 18.63 days). This branching point produces ^{87}Rb directly, with $\approx$50% of the flux going to ^{87}Rb if the neutron density is $\gtrsim 10^{10}$ cm^{-3} (see also Lugaro & Chieffi 2011).

In summary, if the branching points at ^{85}Kr and ^{86}Rb are open ^{87}Rb is produced. This nucleus has a magic number of neutrons of 50 and a low Maxwellian-averaged neutron capture cross-section of 15.7 mbarn at a thermal energy of 30 keV, as compared to 234 for ^{85}Rb (Heil et al. 2008). This means that if ^{87}Rb is produced, it tends to accumulate. Therefore, the $^{87}Rb/^{85}Rb$ isotopic ratios is a direct probe of the neutron density at the production site. It is not possible to distinguish individual

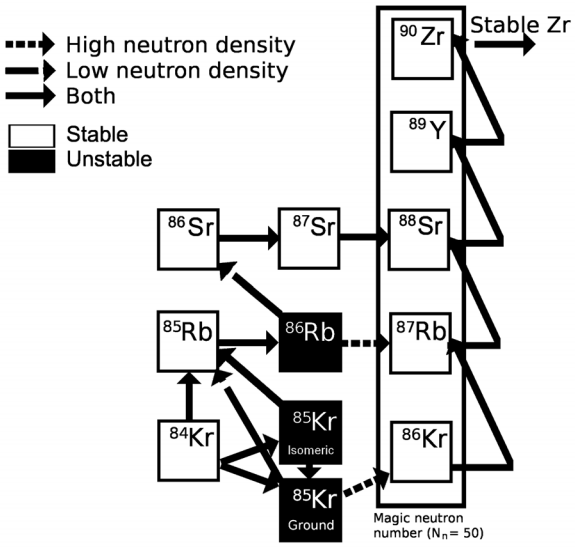

Fig. 1. The *s*-process path in the region of interest in the chart of the nuclides. Isotopes represented by white boxes are stable, isotopes represented by black boxes are unstable. The black arrows indicate the *s*-process path. The solid arrows indicate the *s*-process path branches specific to low neutron densities. The dashed arrows indicate the *s*-process path branches followed under high neutron densities. The rectangular box encircles isotopes with magic neutron number $N = 50$. These isotopes have relatively small neutron capture cross sections.

^{87}Rb and ^{85}Rb from stellar spectra[2] (Lambert & Luck 1976; García-Hernández et al. 2006). However, it is possible to determine the elemental Rb abundance in relation to other neighbouring *s*-process elements, for example Sr, Y, or Zr. This ratio is usually expressed relative to solar and in a logarithmic scale: [Rb/Zr] or [Rb/Sr][3]. A positive/negative [Rb/Zr] or [Rb/Sr] ratio implies a high/low neutron density at the *s*-process production site. This fact has already been used to conclude that the neutron density in M, MS, and S stars must be low, and that the $^{13}C(\alpha, n)^{16}O$ reaction must be the main neutron source in these stars (Lambert et al. 1995). Theoretical models predict that the activation of the ^{22}Ne neutron source and the maximum value of the neutron density are expected to be related to the AGB stellar mass. For this reason the [Rb/Zr] ratio in AGB stars is also predicted to be positively correlated with the initial mass. Using this argument Abia et al. (2001) concluded that C stars must be AGB stars of relatively low mass, <3 $M_\odot$.

Intermediate-mass AGB stars over $\gtrsim$4 $M_\odot$ also experience "hot bottom burning" (HBB). This occurs during the interpulse phase when the convective envelope extends so far inward that it touches the H-burning shell and allows proton-capture reactions to take place at the bottom of the envelope. The CN cycle is activated, which converts ^{12}C into ^{14}N and keeps C < O in the AGB envelope by reducing the C content. Another consequence of HBB is the production of lithium (Li) in form of ^7Li via the Cameron-Fowler mechanism (Cameron & Truran 1977; Boothroyd et al. 1993). This happens via activation of the $^4He(^3He,\gamma)^7Be$ reaction at the base of the envelope, followed by transport of ^7Be towards the stellar surface. There, ^7Be turns into ^7Li via electron captures while the destruction of ^7Li by proton capture is inhibited by the low temperatures. Models of

[2] Though they can be measured in the interstellar medium (Federman et al. 2004).

[3] $[X/Y] = \log_{10}(X/Y) - \log_{10}(X_\odot/Y_\odot)$.

intermediate-mass AGB stars find that the stars become Li-rich during the first ∼10 TPs (Sect. 4.4). Hence, an enhanced Li abundance can be interpreted as a signature of the AGB star being massive (Smith & Lambert 1990)[4].

Studies of intermediate-mass AGB stars in our Galaxy and in the Magellanic Clouds (OH/IR stars, García-Hernández et al. 2006, 2007, 2009) have yielded the first abundances of Rb, Zr, and Li in these stars. The aims of this paper are twofold. First we compare our predictions of Rb and Zr production in intermediate-mass AGB stars to the observations in order to reconfirm that the ^{22}Ne$(\alpha, n)^{25}$Mg reaction is the main neutron source. Second, we try to use the abundances of Rb, Zr, and Li and their observational trends (e.g., Rb increases with increasing stellar mass and/or decreasing metallicity) to constrain the uncertainties in the stellar modelling of intermediate-mass AGB stars. From our detailed comparison we will attempt to define which stellar modelling uncertainties (or other uncertainties e.g., model atmospheres) play the largest role in the apparent mismatch between observations and theory. We will also discuss possible directions for future work to study these problems in more detail.

2. Observations

The studies of the brightest OH/IR AGB stars in our Galaxy and in the Magellanic Clouds by García-Hernández et al. (2006, 2007, 2009) showed that these stars are extremely Rb rich but not Zr rich. This suggests that the ^{22}Ne$(\alpha, n)^{25}$Mg reaction must be the dominant neutron source in intermediate-mass AGB stars.

The mass of the observed stars can be estimated from the observed Mira pulsation period if the distance to the star is known (see, e.g., Wood et al. 1983). For the stars in the Magellanic Clouds this comparison indicated masses of at least 6–7 $M_{\odot}$ (García-Hernández et al. 2009). For the observations of Galactic stars of García-Hernández et al. (2006, 2007) the distance is unknown. However, the Mira pulsation period for these stars shows a correlation with the OH expansion velocity ($v_{\rm exp}$(OH)) Independently for this sample, the correspondence of the $v_{\rm exp}$(OH) with mass is obtained using the location of the observed stars with respect to the Galactic plane. (See Sects. 5.2 and 5.3 of García-Hernández et al. 2007, for a full discussion on the estimation of mass from $v_{\rm exp}$(OH).) From the relationship between $v_{\rm exp}$(OH) and the [Rb/Fe] ratio García-Hernández et al. (2006) estimated that the [Rb/Fe] ratio increases with the initial stellar mass (see their Fig. 2). For the same sample of stars García-Hernández et al. (2007) also measured the Li abundances and found large variations with log(Li/H)+12 ranging from −1.0 to 2.6.

In Table 1 we summarize the Rb and Zr abundances observed in low-mass and intermediate-mass Galactic and Magellanic Cloud AGB stars. The putative low-mass stars in the Magellanic Cloud reported in Table 1 indicated in brackets are the stars observed by Plez et al. (1993) in the Small Magellanic Cloud and the stars classified as "HBB-AGB" in Table 1 of García-Hernández et al. (2009). These stars are poor in Rb, but rich in Li, with log(Li/H) + 12 between +1.9 and +3.5 (Plez et al. 1993). This composition indicates the activation of HBB but not of the ^{22}Ne neutron source. These stars may be more appropriately considered as a link between low-mass Rb-poor and intermediate-mass Rb-rich AGB stars in the Magellanic Clouds. We will discuss these stars against model predictions in Sect. 4.4. Table 1 of García-Hernández et al. (2009) also reported two "Non-HBB-AGB" stars, which have abundances consistent with the values reported in Table 1 for putative low-mass AGB in the Magellanic Clouds, except that one has [Rb/Zr] > 0.3. We note that the distance to the Magellanic Clouds makes even the brightest AGB stars faint, thus they are very challenging to observe with even the VLT. This means that there are only a few observations of intermediate-mass AGB stars in the Magellanic Clouds (e.g., Wood et al. 1983; Smith & Lambert 1990; García-Hernández et al. 2009). Note that in the sample of García-Hernández et al. (2009) there are Rb abundances for only four stars in the Large Magellanic Cloud and one in the Small Magellanic Cloud. These few stars may represent the first truly massive extragalactic AGB stars, as indicated by their strong Rb I lines. On the other hand, the Galactic sample of intermediate-mass AGB stars is much more extensive (120 sources were studied by García-Hernández et al. 2006, 2007). The main trend derived by García-Hernández et al. (2009) by comparing the Galactic to the Magellanic Cloud stars is that higher Rb production is observed in lower metallicity environments, with roughly [Rb/Fe] > 3 in the Large Magellanic Cloud, and [Rb/Fe] < 3 in their Galactic counterparts.

Overall, in low-mass stars the [Rb/Zr] abundance is negative, while in intermediate-mass stars it is positive. This is in qualitative agreement with the current theoretical scenario for the *s* process in AGB stars. Note that the [Rb/Fe] observed in intermediate-mass AGB stars has a large uncertainty of ±0.8 dex, which reflects the sensitivity of the Rb abundance to changes in the atmospheric parameters ($T_{\rm eff}$, gravity,

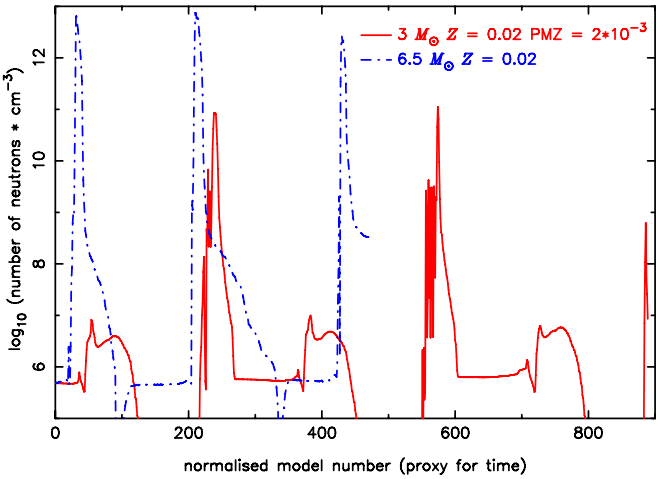

Fig. 2. Maximum neutron density in the He intershell versus normalised model number (proxy for time) showing the last three TPs computed for a 3 $M_{\odot}$ AGB star with a PMZ of 2 ×10^{-3} $M_{\odot}$ (red curve) and a 6.5 $M_{\odot}$ model without a PMZ included (blue curve). The peaks are a result of the ^{22}Ne$(\alpha, n)^{25}$Mg reaction activated during TPs. For the 3 $M_{\odot}$ model the neutron flux during each TPs lasts for ∼4 yr and the total time-integrated neutron flux (neutron exposure τ) is ∼0.02 mbarn^{-1}. In the 6.5 $M_{\odot}$ model the neutron density reaches 10^9 cm^{-3} for ∼3 yr and $\tau \sim 0.2$ mbarn^{-1}. The secondary bumps at ∼10^7 cm^{-3} in the 3 $M_{\odot}$ model are a result of the ^{13}C$(\alpha, n)^{16}$O reaction, which is activated during the interpulse phase due to the PMZ. This activation lasts for ∼30 000 yr and results in $\tau \sim 0.4$ mbarn^{-1} (see also Lugaro et al. 2003). The plateaux at ∼10^6 cm^{-3} represent neutrons released during radiative shell He burning in the interpulse periods. These neutron fluxes are insignificant compared to the others (with $\tau < 0.02$ mbarn^{-1}). Furthermore, the material affected does not make it to the stellar surface as it remains buried in the C–O core. (This figure is available in color in the electronic form.)

[4] Also ∼10% of C-rich AGB stars are Li rich (Abia et al. 1993), which points to the occurrence of some kind of "extra mixing" below the formal border of the convective envelope in low-mass AGB stars.

Table 1. Ranges of the observed Rb and Zr abundances in AGB stars in the Galaxy and in the Magellanic Clouds.

	Putative low-mass AGB stars		Putative intermediate-mass AGB stars	
	Galaxy	Magellanic Clouds[a]	Galaxy	Magellanic Clouds
[Rb/Fe[b]]	−0.3–+0.9	(−1.2–+0.4)	+0.4–+2.5	+1.7–+5.0
[Zr[c]/Fe[b]]	−0.3–+1.4	(−0.3–+0.70)	0[d]	0[d]
[Rb/Zr]	<0	(<0)	>0	>0
[Fe[b]/H]	−1.3–+0.1	(−0.70–−0.37[e])	set to 0[e]	set to −0.3[e] and −0.7[e]
	Lambert et al. (1995) Abia et al. (2001)	Plez et al. (1993) García-Hernández et al. (2009)	García-Hernández et al. (2006) García-Hernández et al. (2007)	García-Hernández et al. (2009)

Notes. [(a)] As discussed in the text, these stars have high Li abundances and may represent a link between low-mass and intermediate-mass AGB stars in the Magellanic Clouds. [(b)] In some of the reported studies the average of Fe and Ni, M, is used instead of Fe. [(c)] In Lambert et al. (1995) [*s*/M] is reported as the average of several *s*-process elements. We use this value as an indicator of the [Zr/Fe] ratio for stars from this study. [(d)] The observational uncertainties allow for an upper limit of +0.5 and of +0.3 for Galactic and Magellanic Clouds intermediate-mass AGB stars, respectively. [(e)] In the studies by Garcia-Hernandez et al., the metallicity of each star is not reported and the Rb and Zr abundances are derived using model atmospheres for the average abundances [M/H] set to 0, −0.3, and −0.7 in the Galaxy, Large and Small Magellanic Clouds, respectively.

etc.) adopted for the modelling (García-Hernández et al. 2006). The observational uncertainties allow for an upper limit of [Zr/Fe] $\lesssim$ 0.5 for Galactic AGB stars, and [Zr/Fe] $\lesssim$ 0.3 for the Magellanic Cloud intermediate-mass AGB stars. By error propagation, the [Rb/Zr] ratios have maximum error bars of ±1.0 dex. We refer the reader to the literature sources indicated in Table 1 for more information on the abundance derivations and their related error bars.

Serious problems are present in current models of the atmospheres of AGB stars. These models are performed in 1D and do not include important effects such as the presence of a circumstellar dust envelope and dust formation. Furthermore, abundance corrections resulting from non local thermodynamic equilibrium (NLTE) need to be taken into account. To our knowledge, such abundance corrections for Rb do not exist in the literature, nevertheless we offer a few comments on NLTE. As for most, if not all, NLTE calculations, missing atomic data may be an issue for Rb. Although NLTE Rb corrections have not yet been established, some expected behaviors may be anticipated based on NLTE corrections for other alkali metals such as Li, Na, and K (e.g. Plez et al. 1993; Asplund 2005; Lind et al. 2011). In fact, for Li and Na Lind et al. (2011) noted "many striking similarities between the two elements, especially in the shape of the abundance correction curves". For Na, the maximum NLTE correction is about 0.70 dex. If the NLTE Rb corrections mimic the behavior for Li and Na, we may therefore expect (a) resonant scattering to be the dominant NLTE mechanism; (b) the NLTE correction to be negative; and (c) the magnitude of the NLTE correction to reach a maximum for saturated lines. The observed Rb abundances in intermediate-mass AGB stars come from strongly saturated Rb I lines and therefore the NLTE Rb abundances would be expected to be smaller, although the exact magnitude of such NLTE Rb corrections have yet to be established. We note that Plez et al. (1993) concluded that NLTE Rb effects in the stars they analysed are likely to be small.

With regard to the 3D hydrodynamical models, the temperature-sensitive Rb I resonance lines originate not only from the photosphere of these stars but also in the outer nonstatic layers of the stellar atmosphere and in the expanding circumstellar shell (García-Hernández et al. 2006). Recent years have seen a rapid development of numerical 3D radiative hydrodynamic simulations of stellar surface convection (see e.g., Collet et al. 2011, and references therein). In these simulations, gas flows in the highly stratified outer layers of stars are modelled by solving the hydrodynamic equations of mass, momentum, and energy conservation and accounting for the energy exchanges between matter and radiation via radiative transfer. In this framework, convective motions arise and self-organize naturally without the need to introduce adjustable parameters. One of the main goals of 3D modelling of stellar surface convection is therefore to provide a more realistic description of the physical structure of late-type stellar atmospheres. From the point of view of spectroscopic analyses, the structural differences between 3D and hydrostatic (1D) models can lead to large differences in terms of derived abundances whenever temperature-sensitive spectral features are used (Asplund 2005). In short, 3D modelling shows that 3D effects are more important at low metallicity and low gravities. This means that the Rb abundances obtained from the sensitive-temperature Rb I resonance lines would be higher in the hydrostatic models compared with the 3D hydrodynamical models as a consequence of the higher temperature in the static case, since the strength of the Rb I resonance lines increases with decreasing temperature (García-Hernández et al. 2006). We would expect drastic 3D effects in intermediate-mass AGB stars at low metallicity. In summary, possible NLTE and 3D Rb corrections could decrease the Rb abundances derived from hydrostatic LTE models by (at least) one order of magnitude. However, these speculations need to be confirmed by detailed 3D hydrodynamical simulations and NLTE calculations.

3. Stellar models

We calculate the nucleosynthesis with a detailed post-processing code (Cannon 1993) for which the stellar evolution inputs were calculated beforehand. The stellar evolution models are from Karakas & Lattanzio (2007) and were calculated with the Monash version of the Mount Stromlo Stellar Structure Program (see Frost & Lattanzio 1996, and references therein for details) with AGB mass loss based on the formula by Vassiliadis & Wood (1993). The choice of mass loss is one of the most important uncertainties in the computation of stellar evolution and it affects the nucleosynthesis by determining the stellar lifetime, which in turn changes the amount of TDU episodes as well as the timescale for the operation of HBB. Another important stellar model uncertainty is the treatment of convection and of convective borders. In our code we use the mixing length theory to parametrize convection with the free parameter α set to the value of 1.75. A different parametrization of convection and a different choice of the mass loss have been shown to have an important impact on the operation of HBB and the resulting AGB yields (Ventura & D'Antona 2005a,b). Furthermore, the treatment of convective boundaries affects the efficiency of the TDU

Table 2. Details of stellar models.

Mass	Z	TPs[a]	$T_{\rm He}^{\rm max}$ (MK)	$T_{\rm bce}^{\rm max}$ (MK)	$M_{\rm dred}$ ($M_\odot$)	Final $M_{\rm env}$ ($M_\odot$)	HBB	C/O	^{12}C/^{13}C
3 $M_\odot$	0.02	26 + 0	302	6.75	0.081	0.676	No	1.40	117.47
4 $M_\odot$	0.02	18 + 2	332	22.7	0.056	0.958	No	0.99	76.22
5 $M_\odot$	0.02	24 + 5	352	64.5	0.050	1.500	Yes	0.77	7.83
6 $M_\odot$	0.02	438 + 5	369	83.1	0.058	1.791	Yes	0.38	10.65
6.5 $M_\odot$	0.02	40 + 7	368	86.5	0.047	1.507	Yes	0.34	9.76
6.5 $M_\odot$	0.012	52 + 2	369	90.0	0.065	1.389	Yes	0.75	10.40
5 $M_\odot$	0.008	59 + 4	366	80.8	0.17	1.795	Yes	0.93	7.49
6 $M_\odot$	0.008	69 + 5	374	89.6	0.12	1.197	Yes	1.41	8.88
4 $M_\odot$	0.004	30 + 2	366	66.3	0.11	1.333	Yes	3.18	7.98
5 $M_\odot$	0.004	83 + 3	377	84.4	0.22	1.141	Yes	2.59	7.88

Notes. [(a)] $+n$ Refers to the number of synthetic TPs as described in Sect. 3.1.

(e.g. Frost & Lattanzio 1996). Here, we apply the Schwarzschild criterion and then extend the convective zone to the neutral border in the same way as described in Lattanzio (1986).

The post-processing code calculates the abundances due to convective mixing and nuclear reaction rates for a large number of species. We use a nuclear network of 166 species from neutrons and protons to S and from Fe to Nb. The missing species are accounted for by means of artificial neutron sinks. For one specific model, the 6 $M_\odot$ $Z = 0.02$, we tested the results produced using a full nuclear network of 320 species and no neutron sinks and found no differences (to within 0.1 dex) for [Rb/Fe], [Zr/Fe], and [Rb/Zr]. The bulk of our 1285 reaction rates are from reaclib (Thielemann et al. 1986), with updated tables as described by Lugaro et al. (2004) and Karakas et al. (2006) in particular for the ^{22}Ne$(\alpha, n)^{25}$Mg reaction. We further updated the neutron capture rates to those of Bao et al. (2000).

We have used here the same stellar models presented by Lugaro et al. (2007) to compare to the composition of peculiar stardust spinel grain OC2 and by Karakas et al. (2009) to compare to the observations of heavy elements in planetary nebulae of Type I. The $Z = 0.008$ and $Z = 0.004$ models were also already used by García-Hernández et al. (2009) to compare to the observations of intermediate-mass Rb-rich O-rich AGB stars in the Magellanic Clouds.

A summary of the properties of the models is given in Table 2, including the mass (Mass) and metallicity (Z) of the model, the number of TPs (TPs), the maximum temperature achieved in the TPs ($T_{\rm He}^{\rm max}$), the maximum temperature achieved at the base of the convective envelope ($T_{\rm bce}^{\rm max}$), the total mass dredged-up to the surface by the TDU ($M_{\rm dred}$), the final envelope mass at the end of the computed evolution ($M_{\rm env}$), if HBB is at work, and the final C/O and ^{12}C/^{13}C ratios.

The observations of García-Hernández et al. (2006) and García-Hernández et al. (2007) are of Galactic-disk AGB stars, and for this reason we concentrated on models of solar metallicity $Z = 0.02$ for masses 3, 4, 5, 6, and 6.5 $M_\odot$. The initial abundances were taken from Anders & Grevesse (1989). We also calculated a 6.5 $M_\odot$ model using the solar abundances from Asplund (2005) and Lodders (2003), which prescribe a solar metallicity of $Z = 0.012$. We further calculated low metallicity models of 6 $M_\odot$ $Z = 0.008$, 5 $M_\odot$ with $Z = 0.008$, and 4 and 5 $M_\odot$ with $Z = 0.004$ which are suitable for comparison to the Magellanic Cloud AGB stars. For the low-metallicity models we used the Anders & Grevesse (1989) abundances scaled down to the appropriate Z.

In four selected models we artificially included a PMZ in the top layers of the intershell in the same way described in detail by Lugaro et al. (2004). For the 3 $M_\odot$ model we used a PMZ of size 2×10^{-3} $M_\odot$. For the 4, 5, and 6.5 models we used a PMZ of size 1×10^{-4} $M_\odot$. This smaller value is because the mass of the intershell is about one order of magnitude smaller in the higher than in the lower mass AGB stars ($\sim 10^{-3}$ $M_\odot$ with respect to $\sim 10^{-2}$ $M_\odot$), so we scaled the mass of the PMZ accordingly. The inclusion of a PMZ is the main uncertainty in models of the *s* process. We still do not know the mechanism and the features of the process driving the mixing, although some promising candidates have been proposed (see Busso et al. 1999, for a discussion). Stellar models of intermediate-mass AGB stars indicate that any protons mixed into the He-intershell during the TDU would likely burn to ^{14}N instead of producing ^{13}C owing to the high temperatures at the base of the envelope (Siess et al. 2004; Herwig 2004). This would inhibit the release of neutrons by the ^{13}C neutron source. For this reason, the artificial inclusion of a PMZ into a model of an intermediate-mass AGB star should be treated with some caution.

3.1. Late AGB-phase evolution

Owing to convergence difficulties, the stellar evolution models used as input into the post-processing calculations were not evolved through to the end of the superwind phase[5] and into the post-AGB phase. That the stellar models have some remaining envelopes (see Table 2) means that there could be further TPs and TDU events (Karakas & Lattanzio 2007). These latest stages of AGB star evolution are pivotal to the abundances under study here. Not only are the observed AGB stars in their late stages of evolution, but the freshly synthesized isotopes from the stellar interior are less diluted inside the rapidly decreasing envelope. To calculate the surface abundance evolution during the final stages of AGB evolution, we use a synthetic patch that we run after the nucleosynthesis code has finished. We estimate the remaining number of pulses based on the stellar parameters during the final time step that was calculated by the stellar evolution code, as described in detail by Karakas & Lattanzio (2007). The number n of remaining pulses for each model are reported in Table 1 as $+n$ in Col. 3. For example, we estimate that 5 and 7 more TP will occur for the 6 $M_\odot$ and 6.5 $M_\odot$, $Z = 0.02$ models, respectively.

The most crucial component for our purposes in these calculations is the TDU efficiency as a function of the decreasing envelope mass. The TDU efficiency λ is defined as the

[5] The superwind is the final stage of the AGB phase when very high mass loss, up to 10^{-4} $M_\odot$/yr (Iben & Renzini 1983) may occur.

Table 3. Final envelope abundances and ratios involving Rb, Zr, the isotopes of Rb, and Li for all our computed models.

M	Z	PMZ mass ($M_\odot$)	Pulse	[Rb/Fe]	[Zr/Fe]	[Rb/Zr]	[^{87}Rb/^{85}Rb]	log(Li/H) + 12
3 $M_\odot$	0.02	0	26	0.00	0.00	−0.01	0.00	1.51
3 $M_\odot$	0.02	2×10^{-3}	26	0.50	1.00	−0.49	−0.11	1.51
4 $M_\odot$	0.02	0	18	0.01	0.01	0.00	0.01	1.30
	extended		20	0.03	0.03	0.00	0.02	
4 $M_\odot$	0.02	1×10^{-4}	18	0.57	0.79	−0.22	0.08	1.18
	extended		20	0.83	1.21	−0.38	0.15	
5 $M_\odot$	0.02	0	24	0.05	0.01	0.03	0.07	2.27
	extended		29	0.33	0.16	0.17	0.37	
5 $M_\odot$	0.02	1×10^{-4}	24	0.39	0.40	−0.01	0.37	2.37
	extended		29	0.80	0.84	−0.04	0.63	
6 $M_\odot$	0.02	0	38	0.21	0.07	0.14	0.25	1.06
	extended		43	0.73	0.46	0.27	0.61	
6.5 $M_\odot$	0.02	0	40	0.26	0.09	0.16	0.30	0.93
	extended		47	1.04	0.73	0.31	0.69	
6.5 $M_\odot$	0.012	0	52	0.22	0.07	0.15	0.25	−0.49
	extended		54	0.69	0.36	0.33	0.56	
6.5 $M_\odot$	0.012	1×10^{-4}	52	0.62	0.60	0.02	0.59	−1.03
	extended		54	1.04	1.04	0.00	0.76	
5 $M_\odot$	0.008	0	59	0.71	0.34	0.37	0.52	−0.33
	extended		63	1.30	1.02	0.29	0.76	
6 $M_\odot$	0.008	0	69	0.90	0.51	0.39	0.60	−0.50
	extended		74	1.44	1.10	0.34	0.77	
4 $M_\odot$	0.004	0	30	0.80	0.28	0.52	0.46	2.98
5 $M_\odot$	0.004	0	83	1.12	1.08	0.04	0.21	−2.68
	extended		86	1.38	1.45	−0.08	0.26	

Notes. The rows labelled as *extended* report the final results obtained using the simple synthetic extension of the evolution described in Sect. 3.1.

fraction of the mass that is dredged up over the mass by which the H-exhausted core had increased in the previous interpulse period, i.e., $\lambda = \frac{\Delta M_{\rm DUP}}{\Delta M_{\rm core}}$. The TDU efficiency in these final phases when the envelope is decreasing could range from $\lambda = 0$ (Straniero et al. 1997) to $\lambda_{\rm max} \approx 0.9$, as in the last TP (Stancliffe & Jeffery 2007; Karakas 2010). In our case these (maximum) efficiencies are: $\lambda = 0.93$, 0.95, and 0.94, for models of 5, 6, and 6.5 $M_\odot$, respectively. This simple synthetic extension of the evolution does not take into account the effect of HBB. However in all cases HBB has ceased in the detailed stellar evolution calculations. The Li abundance is not expected to vary significantly at this stage, owing to the depletion of the ^{3}He fuel needed for Li production and the cessation of HBB.

4. Results

Figure 2 shows the maximum neutron density in the He intershell calculated for two of our models, a low-mass and a intermediate-mass AGB star, as a function of normalised model number (proxy for time). As anticipated, the maximum neutron density from the activation of the ^{22}Ne neutron source is up to two orders of magnitude higher in the intermediate-mass AGB than in the low-mass AGB model, where instead the ^{13}C is the main neutron source. This results in positive and negative [Rb/Zr] in the two models, respectively.

Our results for Rb, Zr, and Li are summarised in Table 3 and illustrated in Figs. 3–6. As reference for future observations, in Table 4 we present the results for a set of key light elements (C, N, O, Na, and Mg) and the Mg isotopic ratios. Inclusion of a PMZ does not significantly affect the results for the light elements, except for the [Na/Fe] ratio in the 3 $M_\odot$ and 4 $M_\odot$ models with $Z = 0.02$, which increases by roughly +0.14 dex with the inclusion of the PMZ (see also Goriely & Mowlavi 2000). Some examples of the effect on the light elements of the synthetic extension of the models are also reported in Table 4. The yields of elements up S for a large range of stellar models, including those presented here, have been published in Karakas (2010) and results for Zn, Ge, Se, Br, and Kr are published in Karakas et al. (2009).

We predict an increase in [Rb/Fe] with increasing stellar mass, as is implied by the observations. This is because a higher stellar mass leads to (i) hotter temperatures during He-shell burning and a stronger activation of the ^{22}Ne neutron source. This results in *s*-process enhancements of [Rb,Zr/Fe] in models more massive than 4 $M_\odot$ even without the inclusion of the PMZ. Also, (ii) a higher number of TPs with high He-burning temperatures and followed by efficient TDU episodes (Table 1). However, intermediate-mass AGB models without synthetic extensions or PMZs produce [Rb/Fe] ratios that do not match the observed values, while the predicted [Zr/Fe] ratios are within the observed range (<0.5, Fig. 3).

We included a PMZ of 1×10^{-4} $M_\odot$ in our calculations for the 5 $M_\odot$, $Z = 0.02$ and 6.5 $M_\odot$, $Z = 0.012$ models and found that [Rb/Fe] increases by a factor of 2 to 3. However, [Zr/Fe] also increases by similar factors. This results in [Rb/Zr]$\sim$ 0, lower than found without the inclusion of a PMZ (Fig. 4). A PMZ in intermediate-mass AGB stars may not provide a solution to the Zr and Rb abundances investigated here.

In comparison with the 5 $M_\odot$ models presented by Abia et al. (2001), we obtain lower production factors for Rb and Zr. This may be due to the different choice of mass-loss rate. Abia et al. (2001) used the prescription by Reimers (1975) with a choice of the free parameter $\eta = 10$, while we used the prescription of Vassiliadis & Wood (1993). However, Table 1 of Straniero et al. (2000) indicates that the 5 $M_\odot$ models used in Abia et al. (2001) experienced 23 TPs, very close to the number in our model.

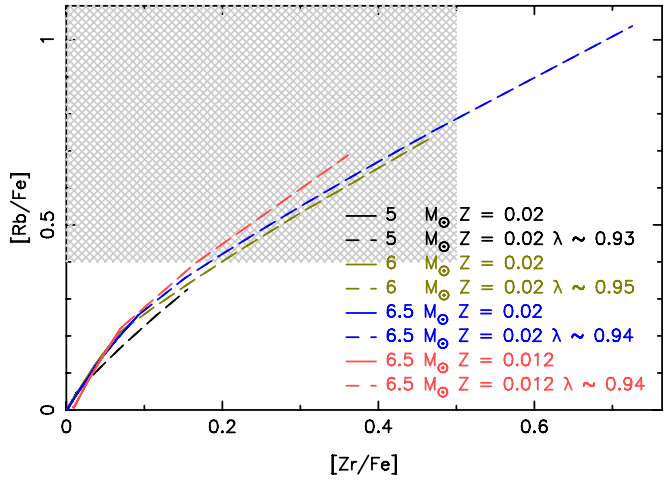

Fig. 3. Model results for the [Rb/Fe] against [Zr/Fe] for intermediate-mass AGB stars of solar metallicity without the inclusion of a PMZ. The solid part of the lines are equivalent to a TDU efficiency of 0 during the extended evolution. The dashed lines are the result of the synthetic extension when the TDU efficiency is chosen to remain constant. The observed [Rb/Fe] and [Zr/Fe] ranges are indicated by the grey shaded area, note that [Rb/Fe] ranges up to 2.5 (±0.8, see Table 1). (This figure is available in color in the electronic form.)

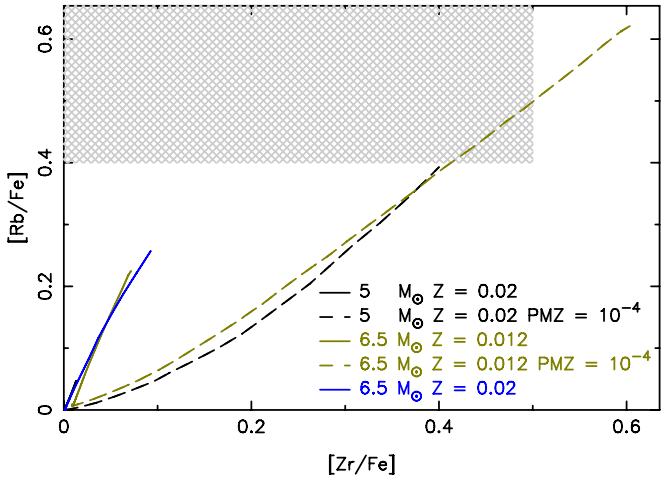

Fig. 4. Results for selected intermediate-mass AGB models with and without the inclusion of PMZs. The solid lines represent model predictions without the inclusion of a PMZ, the dashed line models with a PMZ of 1×10^{-4} $M_{\odot}$. The observed [Rb/Fe] and [Zr/Fe] ranges are indicated by the grey shaded area, note that [Rb/Fe] ranges up to 2.5 (± 0.8, see Table 1). (This figure is available in color in the electronic form.)

The difference must be due to a different ^{13}C abundance in their PMZ. From comparison of the low-mass models we derive that the results from our 3 $M_{\odot}$ AGB model are in agreement with the 1.5 $M_{\odot}$ model presented by Abia et al. (2001) when their standard choice of the amount of the ^{13}C neutron source is selected. For their 5 $M_{\odot}$ model, Abia et al. (2001) divide the amount of ^{13}C by a factor of 10, while we divide the extent in mass of the PMZ by a factor of 20, which results in lower abundances. In any case, there is agreement in terms of the [Rb/Zr] ratio both specifically for the 5 $M_{\odot}$ model, as well as in general, since our intermediate-mass AGB models all produce positive values ratios up to +0.4 (except in the 4 $M_{\odot}$ $Z = 0.02$ model with a PMZ included and the 5 $M_{\odot}$, $Z = 0.004$ model), similarly to the models of Abia et al. (2001) (except for one negative value of −0.4 obtained for their specific standard × 2 choice of the ^{13}C amount).

4.1. Synthetic extension of the models

We extended our models to evolve through the superwind phase using the synthetic algorithm described in Sect. 3.1. The resulting abundances are plotted in Fig. 3 (dashed parts of the lines). The solid parts of the curves in Fig. 3 are equivalent to assuming $\lambda = 0$ during the synthetic extension of the models, while the dashed parts of the curves show the results of extending the models using the same dredge up efficiency as during the last computed pulse, i.e., the maximum possible dredge up efficiency. In this case, we find sufficiently high [Rb/Fe] at the final pulse for the 6 $M_{\odot}$ and 6.5 $M_{\odot}$ models to match the lowest range of the observations (within the observational error bar). We re-emphasise that this synthetic extension is a rough estimate. Even in this case we still cannot match the high end of the observed [Rb/Fe] values, i.e., >1.8. These may be accounted for by AGB stars even more massive than 6.5 $M_{\odot}$. Another difficulty is that most likely HBB is shut off in these late phases and hence it is not possible to keep the star oxygen rich as observed because carbon is carried to the surface via the TDU but it is not consumed by proton captures at the base of the envelope (Table 4).

4.2. Reaction rates

Using the 6.5 $M_{\odot}$ and 6 $M_{\odot}$ $Z = 0.02$ models we performed several tests changing the neutron-capture cross sections involved in the production of Rb specifically with the aims of (i) investigating the relative impact of the two branching points at ^{85}Kr and ^{86}Rb on the production of Rb; and (ii) finding the choice of neutron-capture rates, within their uncertainties, that would maximise the Rb production. The neutron-capture cross sections of the unstable isotopes ^{85}Kr and ^{86}Rb are evaluated only theoretically, and the estimates vary roughly by a factor of two (see the `www.kadonis.org` database) thus we multiplied and divided them by a factor of 2. The neutron-capture cross section of ^{86}Kr has been measured both via the activation technique and the Time Of Flight (TOF) technique. The rate recommended by Bao et al. (2000) is based on the activation measurements, however, the TOF measurements are typically higher (up to 70%) than the activation measurements. We made a test multiplying the ^{86}Kr$(n,\gamma)^{87}$Kr cross section by a factor of 2. The neutron-capture cross sections of ^{85}Rb and ^{87}Rb have been recently re-measured by Heil et al. (2008), who confirmed the values of the previous experiments with a high precision. We also made tests with some combinations of the above choices. The overall result is that the [Rb/Zr] ratio increased at most by 0.28 dex, when considering the synthetic extensions of the models and the following combination of test neutron-capture cross sections σ: $\sigma[^{85}\mathrm{Kr}(n,\gamma)^{86}\mathrm{Kr}]/2$, $\sigma[^{86}\mathrm{Kr}(n,\gamma)^{87}\mathrm{Kr}] \times 2$, and $\sigma[^{86}\mathrm{Rb}(n,\gamma)^{87}\mathrm{Rb}] \times 2$.

Given the surprising result that more Rb was produced when the efficiency of the ^{85}Kr branching factor was smaller, we decided to test the differential impact of the ^{85}Kr and the ^{86}Rb branching points on the production of Rb using the 6 $M_{\odot}$ $Z = 0.02$ model. Assuming instantaneous β-decay of ^{85}Kr we obtained [Rb/Fe] +0.14 higher because [^{87}Rb/Fe] decreased by −0.08 dex, but [^{85}Rb/Fe] increased by +0.25 dex. We ascribe this result to the fact that when the ^{85}Kr branching point is open ^{86}Kr is produced, which has an extremely low Maxwellian-averaged neutron-capture cross section of 3.4 mbarn at a thermal energy of 30 keV (Beer 1991), and it accumulates at the expenses of ^{85}Rb and ^{87}Rb. In fact, [^{86}Kr/Fe] decreased by −0.24 dex in this

test case. Assuming instantaneous β-decay of ^{86}Rb we obtained instead [Rb/Fe] −0.08 lower as a consequence of a −0.25 dex lower [^{87}Rb/Fe].

Finally, again using the 6 $M_\odot$ $Z = 0.02$ model, we checked the effect of varying the ^{22}Ne$(\alpha, n)^{25}$Mg reaction rate. When varying the rate between the upper and lower limits described in Karakas et al. (2006) we found variations in [Rb/Zr] of +0.16 dex at most. When using the rate estimated in the NACRE compilation (Angulo et al. 1999), which is up 40% faster than that of Karakas et al. (2006) at typical He-burning temperatures, we found an increase of +0.21 dex in [Rb/Fe] and of +0.07 dex increase in [Zr/Fe], resulting in a +0.14 dex increase in the [Rb/Zr]. We have also computed selected models using the new ^{22}Ne+α reaction rates from Iliadis et al. (2010). The main finding is that with the new rates both [Rb/Fe] and [Zr/Fe] can increase by up to roughly +0.2 dex, in the 6 $M_\odot$ $Z = 0.008$ model, which is one of the models with the highest He-burning temperatures. For the other models the effect is smaller and basically negligible at solar metallicity. The reasons are that (i) the new ^{22}Ne$(\alpha, n)^{25}$Mg rate is not very different from that used in our study; and (ii) the fact that the revised ^{22}Ne$(\alpha, \gamma)^{26}$Mg rate is roughly an order of magnitude lower than that used here is not significant for the *s* process. This is because the amount of ^{22}Ne that burns is very small in any case: at most the ^{22}Ne intershell abundance decreases by a factor of two. Hence, that the two α-capture channels do not need to compete with each other for the ^{22}Ne.

4.3. Low-metallicity models

Figure 5 shows that low-metallicity intermediate-mass AGB stars show significant enhancements of Rb and Zr, even without including the final synthetic pulses (see also Table 3). This is marginally due to the temperature in TPs being slightly higher in these models, and mostly due to the effect of metallicity on the neutron-capture process itself. The neutron flux is proportional to ^{22}Ne/Z and the amount of ^{22}Ne in low-metallicity AGB stars has a strong primary component due to conversion of primary dredged-up ^{12}C into ^{14}N, which is then converted into ^{22}Ne via double-α capture in the TPs. Hence the neutron flux increases with decreasing metallicity because the amount of material that can capture neutrons (both the light element poisons and the ^{56}Fe seeds) is smaller for lower Z. This results in a larger number of free neutrons and a stronger neutron flux. Also in these cases including TDU in the final pulses results in a significant increase in the surface [Rb/Fe], as well as of [Zr/Fe].

4.4. Lithium

The evolution of Li at the stellar surface for our solar metallicity models is shown in Fig. 6. As the mass of the star increases so does the temperature at the base of the convective envelope during the AGB phase (Table 2). As the temperature increases the first effect on the Li abundance noticeable in the 4, 5, and 6 $M_\odot$ models is the destruction of Li by HBB. This is because proton captures on ^{7}Li are already efficient at temperatures around 20 MK for the low density conditions of HBB. These temperatures are lower than those at which the ^{4}He(^{3}He,γ)^{7}Be reaction is activated (around 40 MK for HBB), which is responsible for the production of Li, after electron captures on ^{7}Be. As the temperature at the base of the envelope inreases as the star evolves along the AGB, the Cameron-Fowler mechanism for the Li production begins, leading in all the HBB models to a Li-rich phase where

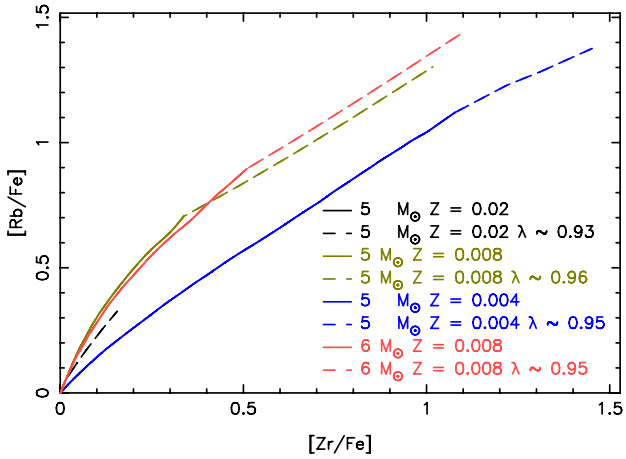

Fig. 5. Resulting [Rb/Fe] and [Zr/Fe] for low-metallicity intermediate-mass AGB models indicated by the labels. For comparison we included the 5 $M_\odot$ $Z = 0.02$ model. As in Fig. 3 the solid part of the lines are equivalent to $\lambda = 0$ during the extended evolution. The dashed lines are the result of the synthetic extension when the TDU efficiency is chosen to remain constant. The observed [Rb/Fe] in five Rb-rich stars in the Magellanic Clouds ranges from +1.7 dex to +5.0 dex, outside of the range of the figure. (This figure is available in color in the electronic form.)

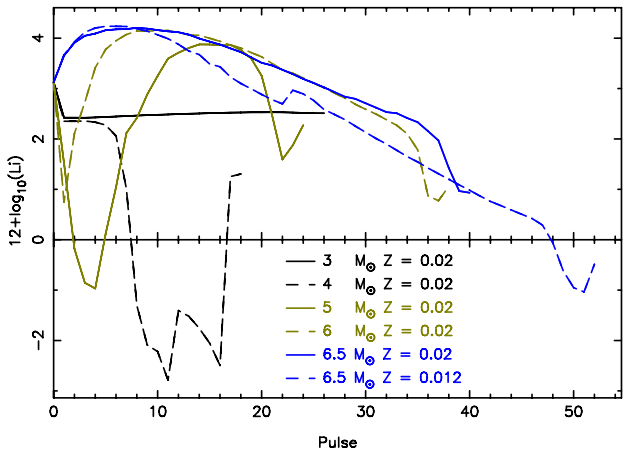

Fig. 6. Li abundance, as log(Li/H) + 12, versus pulse number for our solar-metallicity models. (This figure is available in color in the electronic form.)

the Li abundance reaches a maximum of log(Li/H) + 12 ∼ 4. The Li is mixed to hotter temperatures where it is eventually destroyed by HBB. In our models we find that the Li-rich phase lasts for ≈10^5 years in a 6 $M_\odot$ model. At some point the supply of ^{3}He runs out and Li production by HBB ceases. At this point the star will no longer be observed as Li rich. Our results are in agreement with Li production via HBB presented by Ventura et al. (2000) for models of metallicity 0.01. There, the Li abundance also first decreases, in the models of mass less than ∼6 $M_\odot$, and then reaches a maximum close to log(Li/H) + 12 ∼ 4 before declining to lower values. From Table 3 it can be noted that for a given initial mass, stars of lower metallicity have a lower final Li abundance. This is becasue they reach higher temperature at the base of the convective envelope (see Table 2) and destroy Li more efficiently.

In Fig. 7 we compare predictions for selected models to the observations of stars from García-Hernández et al. (2006) and García-Hernández et al. (2007) for which both Rb and Li data are

Table 4. Same as Table 3 but for abundances and ratios involving C, N, O, Na, Mg and the isotopes of Mg for our computed models without inclusion of a PMZ.

M	Z	[C/Fe]	[N/Fe]	[O/Fe]	[Na/Fe]	[Mg/Fe]	[^{25}Mg/^{24}Mg]	[^{26}Mg/^{24}Mg]
3 $M_\odot$	0.02	0.49	0.34	−0.02	0.19	0.01	0.03	0.03
4 $M_\odot$	0.02	0.34	0.38	−0.02	0.17	0.03	0.10	0.10
5 $M_\odot$	0.02	0.21	0.57	−0.04	0.28	0.04	0.13	0.18
extended		0.60	0.56	−0.05	0.31	0.14	0.41	0.50
6 $M_\odot$	0.02	−0.14	0.89	−0.08	0.85	0.07	0.22	0.31
extended		0.46	0.88	−0.08	0.85	0.20	0.51	0.67
6.5 $M_\odot$	0.02	−0.19	0.87	−0.09	0.79	0.06	0.22	0.30
extended		0.70	0.86	−0.09	0.80	0.32	0.69	0.89
6.5 $M_\odot$	0.012	−0.16	0.87	−0.41	0.64	0.04	0.46	0.38
5 $M_\odot$	0.008	0.19	1.51	−0.14	1.52	0.31	0.59	0.77
6 $M_\odot$	0.008	0.26	1.39	−0.25	1.04	0.28	0.79	0.80
4 $M_\odot$	0.004	0.88	1.57	−0.17	0.93	0.35	0.68	0.92
5 $M_\odot$	0.004	0.56	1.89	−0.22	1.78	0.63	0.83	1.10

Notes. Solar reference ratios are taken from Anders & Grevesse (1989).

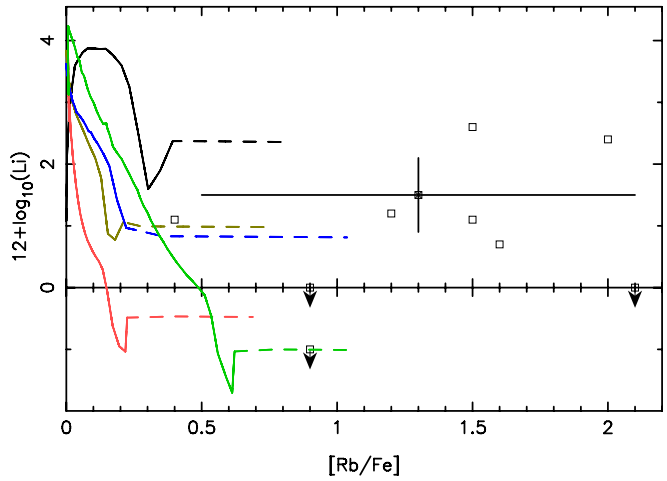

Fig. 7. Li abundance versus [Rb/Fe] observed in intermediate-mass AGB stars (squares) and predicted by our models (solid lines: computed evolution, dashed lines: synthetic evolution as in Figs. 3 and 4). Different line colours indicate the following models: 5 $M_\odot$ Z = 0.02 with PMZ of size 0.0001 $M_\odot$ (black); 6 $M_\odot$ Z = 0.02; (blue) 6.5 $M_\odot$ Z = 0.02 (dark green); 6.5 $M_\odot$ Z = 0.012 (red); 6.5 $M_\odot$ Z = 0.012 with PMZ of 0.0001 $M_\odot$ (light green). The error bars represent the maximum errors for each individual data point, though for sake of clarity they are included for only one data point. Arrows indicate upper limits. (This figure is available in color in the electronic form.)

available. Shown are also the results for [Rb/Fe] for the synthetic extension of the models, which as noted above, do not include possible further decreases of Li. The observations show large variations in qualitative agreement with the large changes in Li seen in the models and due to the strong sensitivity of Li to the temperature of HBB. The stars in the Small Magellanic Clouds observed by Plez et al. (1993) have log(Li/H) + 12 between +1.9 and +3.5 and negative [Rb/Fe], which most likely reflects their initial composition. Our 5 $M_\odot$ model of Z = 0.02 would provide a good fit to these observations because HBB is producing Li and keeping the ^{12}C/^{13}C ratio low, as observed, but without a significant increase in the [Rb/Fe] abundance. However, this metallicity is too high to be compared to the Small Magellanic Clouds. For models at the required Z = 0.004 metallicity Rb production occurs already from the lowest masses at which HBB is activated (e.g., the 4 $M_\odot$ models at this metallicity in Table 3). The stars observed by Plez et al. (1993) either (i) are all stars in the early phases of the thermally-pulsing AGB where Li production is active but the Rb abundance has yet to increase; or (ii) indicate that HBB needs to be more efficient and be activated at masses where no substantial Rb production is expected. This may be achieved by a different description of convection, either via the Full Spectrum of Turbulence or equivalently by using a higher mixing length parameter α (Ventura & D'Antona 2005a).

5. Discussion and conclusions

Our main conclusions can be summarised as follows:

1. We predict an increase in the [Rb/Fe] ratio with increasing stellar mass. This is also suggested by the observations. However, our standard models are not able to quantitatively reproduce the high [Rb/Fe] values found in the observed intermediate-mass OH/IR stars.
2. Inclusion of a partial mixing zone (PMZ) increases the final surface Rb content, but also increases the Zr content, resulting in a [Zr/Fe] that is higher than the observed upper limit.
3. The uncertainties in the neutron-capture cross sections relevant to Rb production do not introduce significant enough changes to our predicted [Rb/Fe] to match the observed data. Varying the ^{22}Ne$(\alpha, n)^{25}$Mg neutron source rate produces modest increases to the [Rb/Fe] ratio, but not enough to match the observed values.
4. In order to remove the whole envelope we synthetically extend our models. By including these final pulses we find [Rb/Fe] ratios that are high enough to match the lower end of the observed data, taking into account the large error bars on the data. This relies on the TDU efficiency remaining as high during the final few TPs as it was at the last computed TP. A better understanding of the TDU efficiency with receding envelope mass is essential and requires further investigation. However, one difficulty is that HBB is expected to be ineffective during this final stage of AGB evolution. This means the star will likely become carbon rich if the TDU is efficient, while the observed stars are oxygen rich.
5. More Rb (in absolute numbers) is produced as the metallicity decreases. This reproduces the observed qualitative trend as derived from recent data for low-metallicity intermediate-mass AGB stars in the Magellanic Clouds (García-Hernández et al. 2009). However, also in this case the models cannot match the observations quantitatively.

The main overall difficulty in matching the Rb and Zr observed abundances is that the *s* process cannot produce differences larger than 0.5 dex between Zr and Rb as these two elements belong to the same *s*-process peak. On the other hand, the observations show differences between these elements up to 5 dex. Since the maximum [Rb/Zr] ratio produced by the *s* process is independent of the stellar models and their uncertainties, as it derives from the basic operation of the *s* process and the neutron-capture cross sections of the nuclei involved (which are know to the level of 5%), we need to turn to observational uncertainties to explain the mismatch for the [Rb/Zr] ratio. As discussed in Sect. 2 and in García-Hernández et al. (2009) the solution to the problem may lie with an incomplete understanding of the atmospheres of luminous AGB stars. More realistic model atmospheres for intermediate-mass O-rich AGB stars (e.g., the inclusion of a circumstellar dust envelope and 3D hydrodynamical simulations) as well as NLTE calculations need to be developed in order to shed some light on the observed discrepancy between the observations and the AGB nucleosynthesis theoretical predictions.

Another possibility that needs to be carefully evaluated is whether the Rb and Zr abundances in these stars are affected by dust condensation. The condensation temperature of Zr in a gas of solar-system composition is 1741 K (Lodders 2003), and it would be even higher in a gas where the abundance of Zr is enhanced by the *s* process. It is reasonable to expect that a significant fraction of the Zr abundance is removed from the gas by condensation into dust. On the other hand, the condensation temperature of Rb is much lower (800 K), and this element is not expected to be removed from the gas. This effect could explain the observations, which samples the gas and not the dust, around the star. A similar idea was put forward by Dinerstein et al. (2006) to explain the non-detection of the ground-state fine-structure line of triply ionized Zr in several planetary nebulae known to have enhanced abundances of other light neutron-capture elements. To explain the most extreme observed [Rb/Zr] ratios requires that most of the Zr and none of the Rb has condensed into dust around these stars. This possibility needs to be examined by detailed models of dust formation.

If this "dust selection" effect is found to be significant, then stellar model uncertainties can also be invoked to play a role in the mismatch between data and predictions with regards to the [Rb/Fe] ratio. For example, the inclusion of a PMZ in intermediate-mass AGB stars may provide a solution to the Rb abundances investigated here, although as discussed in Sect. 3 this would be at odds with the current modelling of the PMZ in intermediate-mass AGB stars. Another complementary solution may be found by increasing the number of TPs and TDUs episodes experienced by the stellar models. This number depends on the mass-loss rate of intermediate-mass AGB stars, which is also highly uncertain. Vassiliadis & Wood (1993) noted that there are optically bright long period variable stars with periods of ≈750 days that are probably intermediate-mass stars of ∼5 $M_{\odot}$. In order to prevent their mass-loss prescription from removing these observed objects, Vassiliadis & Wood (1993) recommend a modification to delay the onset of the superwind in stars of masses greater than 2.5 $M_{\odot}$. Note that in the models presented here we have not used this modification, which would keep the mass-loss rate low for a longer time and would result in more TPs and TDU episodes. It would also keep the envelope mass relatively high, allowing HBB to operate efficiently for more TPs. The outcome would likely be higher levels of Rb (and Zr) production in an O-rich envelope. Also, Rb production in AGB stars with masses greater than 6.5 $M_{\odot}$ need to be computed. Finally, a higher temperature in the TP would lead to higher Rb production. This may be related to the penetration of flash-driven convection deeper into the core due to the inclusion of hydrodynamical overshoot. This would increase the efficiency of the ^{22}Ne neutron source as discussed by Lugaro et al. (2003). Detailed modelling is needed to explore the viability of these scenarios.

Future observations of the isotopic composition of Mg in the stars considered here would provide further observational evidence that the ^{22}Ne neutron source is activated in these stars as the neutron-rich isotopes of Mg, ^{25}Mg and ^{26}Mg are expected to be enhanced due to direct production via the ^{22}Ne+α reactions (Karakas & Lattanzio 2003; Karakas et al. 2006, and Table 4). Several more elements could be measured in AGB stars, and N would be particularly interesting to constrain HBB. Also the derivation of other *s*-process elements, e.g., Ba, La, Ce, and Pb, is possible and could help to further constrain the models. Though the predictions presented here involved a nuclear network up to Nb, we are currently working to extend these models up to Pb. AGB stars have complex atmospheres so which elements can actually be measured depends on the temperature, metallicity, and abundance for each individual star.

Finally, the observations and models discussed here indicate that intermediate-mass AGB stars synthesize large amounts of Rb and that more Rb (in absolute numbers) is produced when lowering the metallicity. From this prediction, we extrapolate that intermediate-mass AGB model of metallicities typical of globular clusters ($Z \sim 10^{-3}$) will produce even larger abundances of Rb than presented here. If intermediate-mass AGB stars produced the heavy elements in globular cluster stars, then this would rule out these stars as candidates for the O, Na, Mg, and Al anomalies. This is because no correlation has been observed between the heavy elements and the light elements in globular cluster stars (Yong et al. 2006, 2008b,a). A preliminary study by Karakas et al. (2010) appears to confirm our predictions on the basis of two intermediate-mass AGB models, however, a larger set of detailed models at the relevant metallicities needs to be calculated. Furthermore, we also need to account for the data of Plez et al. (1993), which indicates that at metallicities appropriate to the Magellanic Clouds there is a mass or evolutionary time when HBB is active but not the ^{22}Ne neutron source. A dedicated analysis of these stars will be the focus of a future work.

Acknowledgements. We thank Carlos Abia and Martin Asplund for discussions. We thank the anonymous referee for a very detailed report, which helped to improve the paper and to broaden the discussion. M.L. is an A.R.C. Future Fellow. A.I.K. is a Stromlo Fellow. D.A.G.H. acknowledges support provided by the Spanish Ministry of Science and Innovation (MICINN) under a JdC grant and under grant AYA-2007-64748.

References

Abia, C., Boffin, H. M. J., Isern, J., & Rebolo, R. 1993, A&A, 272, 455
Abia, C., Busso, M., Gallino, R., et al. 2001, ApJ, 559, 1117
Anders, E., & Grevesse, N. 1989, Geochim. Cosmochim. Acta, 53, 197
Angulo, C., Arnould, M., Rayet, M., et al. 1999, Nuclear Phys. A, 656, 3
Arlandini, C., Käppeler, F., Wisshak, K., et al. 1999, ApJ, 525, 886
Asplund, M. 2005, ARA&A, 43, 481
Bao, Z. Y., Beer, H., Käppeler, F., et al. 2000, Atomic Data and Nuclear Data Tables, 76, 70
Beer, H. 1991, ApJ, 375, 823
Beer, H., & Macklin, R. L. 1989, ApJ, 339, 962
Boothroyd, A. I., Sackmann, I.-J., & Ahern, S. C. 1993, ApJ, 416, 762
Busso, M., Gallino, R., & Wasserburg, G. J. 1999, ARA&A, 37, 239
Busso, M., Gallino, R., Lambert, D. L., Travaglio, C., & Smith, V. V. 2001, ApJ, 557, 802
Cameron, A. G. W., & Truran, J. W. 1977, Icarus, 30, 447
Cannon, R. C. 1993, MNRAS, 263, 817

Collet, R., Hayek, W., Asplund, M., et al. 2011, A&A, 528, A32
Dinerstein, H. L., Lacy, J. H., Sellgren, K., & Sterling, N. C. 2006, in BAAS, 38, Am. Astron. Soc. Meet. Abstracts, 156.09
Federman, S. R., Knauth, D. C., & Lambert, D. L. 2004, ApJ, 603, L105
Frost, C. A., & Lattanzio, J. C. 1996, ApJ, 473, 383
Gallino, R., Arlandini, C., Busso, M., et al. 1998, ApJ, 497, 388
García-Hernández, D. A., García-Lario, P., Plez, B., et al. 2006, Science, 314, 1751
García-Hernández, D. A., García-Lario, P., Plez, B., et al. 2007, A&A, 462, 711
García-Hernández, D. A., Manchado, A., Lambert, D. L., et al. 2009, ApJ, 705, L31
Goriely, S. 1999, A&A, 342, 881
Goriely, S., & Mowlavi, N. 2000, A&A, 362, 599
Heil, M., Käppeler, F., Uberseder, E., et al. 2008, Phys. Rev. C, 78, 025802
Herwig, F. 2004, ApJ, 605, 425
Herwig, F. 2005, ARA&A, 43, 435
Hollowell, D., Iben, I. J., & Fujimoto, M. Y. 1990, ApJ, 351, 245
Iben, Jr., I. 1975, ApJ, 196, 525
Iben, I., J., & Renzini, A. 1983, ARA&A, 21, 271
Iliadis, C., Longland, R., Champagne, A. E., Coc, A., & Fitzgerald, R. 2010, Nuclear Phys. A, 841, 31
Käppeler, F., Beer, H., & Wisshak, K. 1989, Rep. Progress Phys., 52, 945
Karakas, A. I. 2010, MNRAS, 403, 1413
Karakas, A. I., & Lattanzio, J. C. 2003, PASA, 20, 279
Karakas, A., & Lattanzio, J. C. 2007, PASA, 24, 103
Karakas, A. I., Lugaro, M., Wiescher, M., Goerres, J., & Ugalde, C. 2006, ApJ, 643, 471
Karakas, A. I., van Raai, M. A., Lugaro, M., Sterling, N. C., & Dinerstein, H. L. 2009, ApJ, 690, 1130
Karakas, A. I., Campbell, S. W., Lugaro, M., Yong, D., & Chieffi, A. 2010, Mem. Soc. Astron. It., 81, 1010
Lambert, D. L., & Luck, R. E. 1976, The Observatory, 96, 100
Lambert, D. L., Smith, V. V., Busso, M., Gallino, R., & Straniero, O. 1995, ApJ, 450, 302
Lattanzio, J. C. 1986, ApJ, 311, 708
Lind, K., Asplund, M., Barklem, P. S., & Belyaev, A. K. 2011, A&A, 528, A103
Lodders, K. 2003, ApJ, 591, 1220
Lugaro, M., & Chieffi, A. 2011, in Lecture Notes in Physics, ed. R. Diehl, D. H. Hartmann, & N. Prantzos (Berlin: Springer Verlag), 812, 83
Lugaro, M., Herwig, F., Lattanzio, J. C., Gallino, R., & Straniero, O. 2003, ApJ, 586, 1305
Lugaro, M., Ugalde, C., Karakas, A. I., et al. 2004, ApJ, 615, 934
Lugaro, M., Karakas, A. I., Nittler, L. R., et al. 2007, A&A, 461, 657
Meyer, B. S. 1994, ARA&A, 32, 153
Plez, B., Smith, V. V., & Lambert, D. L. 1993, ApJ, 418, 812
Reimers, D. 1975, Circumstellar envelopes and mass loss of red giant stars (New York: Springer-Verlag), 229
Siess, L., Goriely, S., & Langer, N. 2004, A&A, 415, 1089
Simmerer, J., Sneden, C., Cowan, J. J., et al. 2004, ApJ, 617, 1091
Smith, V. V., & Lambert, D. L. 1990, ApJ, 361, L69
Stancliffe, R. J., & Jeffery, C. S. 2007, MNRAS, 375, 1280
Straniero, O., Chieffi, A., Limongi, M., et al. 1997, ApJ, 478, 332
Straniero, O., Limongi, M., Chieffi, A., et al. 2000, Mem. Soc. Astron. Italiana, 71, 719
Thielemann, F.-K., Truran, J. W., & Arnould, M. 1986, in Adv. Nucl. Astrophys., ed. E. Vangioni-Flam, J. Audouze, M. Casse, J.-P. Chieze, & J. Tran Thanh van (Gif-sur-Yvette, France: éditions Frontieres), 525
Travaglio, C., Gallino, R., Arnone, E., et al. 2004, ApJ, 601, 864
Vassiliadis, E., & Wood, P. R. 1993, ApJ, 413, 641
Ventura, P., & D'Antona, F. 2005a, A&A, 431, 279
Ventura, P., & D'Antona, F. 2005b, A&A, 439, 1075
Ventura, P., D'Antona, F., & Mazzitelli, I. 2000, A&A, 363, 605
Wood, P. R., Bessell, M. S., & Fox, M. W. 1983, ApJ, 272, 99
Yong, D., Aoki, W., Lambert, D. L., & Paulson, D. B. 2006, ApJ, 639, 918
Yong, D., Karakas, A. I., Lambert, D. L., Chieffi, A., & Limongi, M. 2008a, ApJ, 689, 1031
Yong, D., Lambert, D. L., Paulson, D. B., & Carney, B. W. 2008b, ApJ, 673, 854